

Dissipative particle dynamics: systematic parametrization using water-octanol partition coefficients

Richard L. Anderson,^{1,*} David J. Bray,¹ Andrea S. Ferrante,^{2,3}
Massimo G. Noro,⁴ Ian P. Stott,⁴ and Patrick B. Warren^{4,†}

¹*STFC Hartree Centre, Scitech Daresbury, Warrington, WA4 4AD, UK*

²*Novidec Ltd., 3 Brook Hey, Parkgate, Neston, CH64 6TH, UK*

³*Ferrante Scientific Ltd., 5 Croft Lane, Bromborough, CH62 2BX, UK*

⁴*Unilever R&D Port Sunlight, Quarry Road East, Bebington, CH63 3JW, UK*

(Dated: June 27, 2017)

We present a systematic, top-down, thermodynamic parametrization scheme for dissipative particle dynamics (DPD) using water-octanol partition coefficients, supplemented by water-octanol phase equilibria and pure liquid phase density data. We demonstrate the feasibility of computing the required partition coefficients in DPD using brute-force simulation, within an adaptive semi-automatic staged optimization scheme. We test the methodology by fitting to experimental partition coefficient data for twenty one small molecules in five classes comprising alcohols and poly-alcohols, amines, ethers and simple aromatics, and alkanes (*i. e.* hexane). Finally, we illustrate the transferability of a subset of the determined parameters by calculating the critical micelle concentrations of selected alkyl ethoxylate surfactants, in good agreement with reported experimental values.

I. INTRODUCTION

In this work we describe a systematic, top-down parametrization scheme for dissipative particle dynamics (DPD) based on matching water-octanol partition coefficients, water-octanol phase equilibria, and pure liquid phase density data. Apart from water, the DPD ‘beads’ in the model represent molecular fragments, and as such can be assembled to cover a wide range of organic materials such as polymers, surfactants, oils, and so on. The resulting DPD parameter set can be used for an equally wide range of applications, and we give the example of calculating the critical micelle concentrations of alkyl ethoxylate surfactants. Our approach is extensible in the sense that it is easy to broaden the molecular ‘palette’, and flexible in the sense that the calculations can be re-run semi-automatically if it is necessary to make different changes to the coarse-graining or include extra moieties or interactions. The remaining manual aspects would be potentially amenable to machine learning approaches. Finally, turned around, our approach offers a potential novel way of calculating partition coefficients for new molecules.

We organize the paper by first describing the partition coefficients that we use as the principal parametrization target. We then explain the coarse-grained DPD model and parametrization strategy. We finally analyze and discuss the results. Technical details of the computational approach are given in a ‘methods’ Appendix, and a further short Appendix discusses compressibility matching in DPD.

II. PARTITION COEFFICIENTS

The partition coefficient of an uncharged solute molecule is the ratio of the molar concentrations in a pair of coexisting bulk phases, at equilibrium. The bulk phases themselves are typically made up from a pair of (near) immiscible solvents, and the corresponding partition coefficient is usually reported as a base 10 logarithm,

$$\log P_{A/B} = \log_{10} \frac{[S]_A}{[S]_B} \quad (1)$$

where $[S]_A$ and $[S]_B$ are the molar concentrations of a solute molecule in the two phases, A and B.

By far the most commonly studied partition coefficient is for the water/octanol system (where octanol means 1-octanol in the present work); hereafter we shall denote this specific partition coefficient as simply $\log P$. The partition coefficient is a measure of the propensity of a solute to partition between hydrophobic and hydrophilic environments, and is widely used across numerous application areas such as toxicology, pharmaceutical drug delivery (pharmacokinetics), and so on [1, 2]. For example, hydrophobic molecules with $1 \lesssim \log P \lesssim 5$ are generally considered to be cytotoxic since they are able to cross hydrophobic cell membranes whilst retaining sufficient water solubility to be active [3].

Given the diverse range of applications, it is not surprising that a large amount of experimental $\log P$ data is available both in the primary literature and in curated databases, for a wide variety of solute molecules [2, 4, 5]. Moreover, diverse numerical methods with varying degrees of sophistication and accuracy have been developed to calculate $\log P$ values, to augment the existing experimental data. These methods include quantitative structure-property relationships (QSPR) [6, 7]; and atom-based [8], and quantum chemistry motivated methods such as COSMOtherm/COSMO-RS [9–11].

* richard.anderson@stfc.ac.uk

† patrick.warren@unilever.com

TABLE I. Coarse-grained (CG) representations of molecules considered in the present work. The CG bead content is denoted by the contents of square brackets.

molecule	SMILES code	# beads	CG mapping
hexane	cccccc	4	$[\text{CH}_3][\text{CH}_2\text{CH}_2]_2[\text{CH}_3]$
octane	ccccccc	5	$[\text{CH}_3][\text{CH}_2\text{CH}_2]_3[\text{CH}_3]$
decane	cccccccc	6	$[\text{CH}_3][\text{CH}_2\text{CH}_2]_4[\text{CH}_3]$
dodecane	ccccccccc	7	$[\text{CH}_3][\text{CH}_2\text{CH}_2]_5[\text{CH}_3]$
tetradecane	ccccccccccc	8	$[\text{CH}_3][\text{CH}_2\text{CH}_2]_6[\text{CH}_3]$
benzene	c1ccccc1	3	$[\text{aCHCH}]_1[\text{aCHCH}][\text{aCHCH}]_1$
ethanol	cco	2	$[\text{CH}_3][\text{CH}_2\text{OH}]$
1-butanol	cccc	3	$[\text{CH}_3][\text{CH}_2\text{CH}_2][\text{CH}_2\text{OH}]$
1-hexanol	ccccco	4	$[\text{CH}_3][\text{CH}_2\text{CH}_2]_2[\text{CH}_2\text{OH}]$
1-octanol	ccccccc	5	$[\text{CH}_3][\text{CH}_2\text{CH}_2]_3[\text{CH}_2\text{OH}]$
butan-1,4-diol	occcco	3	$[\text{CH}_2\text{OH}][\text{CH}_2\text{CH}_2][\text{CH}_2\text{OH}]$
glycerol	c(c(co)o)o	3	$[\text{CH}_2\text{OH}]_3$
tetritol	ccc(c(co)o)o	4	$[\text{CH}_2\text{OH}]_4$
ethylamine	ccn	2	$[\text{CH}_3][\text{CH}_2\text{NH}_2]$
butylamine	cccn	3	$[\text{CH}_3][\text{CH}_2\text{CH}_2][\text{CH}_2\text{NH}_2]$
ethanolamine	ccn	2	$[\text{CH}_2\text{OH}][\text{CH}_2\text{NH}_2]$
diethyl ether	ccoc	3	$[\text{CH}_3][\text{CH}_2\text{OCH}_2][\text{CH}_3]$
glyme	cococ	2	$[\text{CH}_2\text{OCH}_3][\text{CH}_2\text{OCH}_3]$
diglyme	cocccoc	3	$[\text{CH}_3\text{OCH}_2][\text{CH}_2\text{OCH}_2][\text{CH}_3\text{OCH}_2]$
tetraglyme	cocccocccoc	5	$[\text{CH}_3\text{OCH}_2][\text{CH}_2\text{OCH}_2]_3[\text{CH}_3\text{OCH}_2]$
2-hexyloxyethanol	ccccccoco	5	$[\text{CH}_3][\text{CH}_2\text{CH}_2]_2[\text{CH}_2\text{OCH}_2][\text{CH}_2\text{OH}]$
ethyl diglyme	ccocccoc	5	$[\text{CH}_3][\text{CH}_2\text{OCH}_2][\text{CH}_2\text{OCH}_2][\text{CH}_2\text{OCH}_2][\text{CH}_3]$
phenylmethylether	coc1ccccc1	4	$[\text{CH}_3\text{OCH}_2][\text{aCHCH}]_1[\text{aCHCH}][\text{aCHCH}]_1$
phenylpropanol	occc1ccccc1	5	$[\text{CH}_2\text{OH}][\text{CH}_2\text{CH}_2][\text{aCHCH}]_1[\text{aCHCH}][\text{aCHCH}]_1$
phenylpropylamine	nccc1ccccc1	5	$[\text{CH}_2\text{NH}_2][\text{CH}_2\text{CH}_2][\text{aCHCH}]_1[\text{aCHCH}][\text{aCHCH}]_1$
C_nE_m	$[\text{c}]_n[\text{occ}]_m[\text{o}]$	$\frac{1}{2}n + m + 1$	$[\text{CH}_3][\text{CH}_2\text{CH}_2]_{n/2-1}[\text{CH}_2\text{OCH}_2]_m[\text{CH}_2\text{OH}]$

Computer simulations, *e. g.* molecular dynamics (MD) or Monte Carlo (MC) methods using atom-based potential functions or coarse-grained force-fields such as the MARTINI force field [12], provide an additional route to the prediction of $\log P$ for small or medium size solute molecules [13–29]. There have also been attempts to use multiscale simulation methods mixing atomistic and coarse-grained potentials [13, 30]. To our knowledge, all published results to date using these methods resort to the thermodynamically equivalent definition $\log P = -\log_{10} e \times \Delta G_{\text{transfer}}/RT$ where $\Delta G_{\text{transfer}}$ is the Gibbs free energy to transfer one mole of solute from phase A to phase B, and RT is the product of the gas constant R and the temperature T . The transfer free energy can be formally resolved into the difference between solvation free energies for which thermodynamic perturbation and thermodynamic integration methods are typically employed [14–16, 19–26, 31–34].

It is important to note that a direct application of MC methods such as Widom insertion are not usually viable for atomistic and coarse grained simulation methods based on hard core or Lennard-Jones potentials at liquid densities [35, 36]. Also determination of the transfer free energy as the *difference* in solvation free energies may require computing the latter with a high degree of precision and accuracy. This makes these methods very demanding.

In carrying out simulations one could employ pure solvent boxes (*i. e.* pure water and pure octanol), but it is

known that the results for ‘dry’ octanol (*i. e.* pure octanol) may be drastically different from ‘wet’ octanol, since the solubility of water in octanol is considerable and wet octanol better represents the experimental situation [28]. More realistically therefore, one should equilibrate the solvent boxes, and to address this problem one can turn to Gibbs ensemble methods in which MC solvent molecule exchange moves are allowed between two separate simulation boxes. With a Gibbs ensemble method, one can in principle include solute molecules, and directly evaluate $\log P$ as the ratio of solute concentrations using the definition in Eq. (1).

Finally we note that the definition of $\log P$ can be extended to include the molecular components of the solvents themselves. This is because we can imagine labelling a small fraction of a given solvent molecule, and defining its partition coefficient using Eq. (1) where the ratio $[S]_A/[S]_B$ can be replaced by the ratio of the molar compositions in the coexisting phases. For example, in the water-octanol system we can define water and octanol partition coefficients, and use them interchangeably with the mutual solubilities. Obviously this only makes sense for the equilibrated system (*i. e.* ‘wet’ octanol as defined above).

III. COARSE GRAINED MODEL DEFINITION

In our approach the DPD beads represent molecular fragments comprising 1–3 ‘heavy atoms’ (*i. e.* C, O, N in this work), with the exception of water (H₂O) which is treated super-molecularly. This means that a wide variety of both aqueous and non-aqueous systems can be modelled by combining these fragments as a kind of molecular ‘Lego’ game. It also means the approach is extensible, since the molecular palette is easily enlarged.

To establish the basis for the above coarse-graining scheme, we first follow Groot and Rabone in defining a water mapping number, in our case $N_m = 2$ so that each water bead corresponds, on average, to two water molecules. Following well established protocols we also assert that the density of water in our model corresponds to $\rho r_c^3 = 3$ in DPD units. We can then use the mapping number tautology $\rho N_m v_m \equiv 1$, where $v_m \approx 30 \text{ \AA}^3$ is the molecular volume of liquid water (corresponding to a molar volume $\approx 36.0 \text{ cm}^3 \text{ mol}^{-1}$), to determine that $r_c \approx 5.65 \text{ \AA}$. This underpins the conversion of all lengths and molecular densities in the model.

In our model, alkane molecules are constructed from connected (bonded) beads comprising (i) CH₂CH₂ groups of atoms and (ii) CH₃, a terminal methyl group. Similarly alcohol molecules are constructed by bonding together alkane beads and a specific bead containing an alcohol functionality, *e. g.* comprised of the CH₂OH group of atoms. Amine molecules follow the same model definition where the amine functionality is captured in a bead comprised of CH₂NH₂ atoms. Benzene rings are constructed from a total of three beads, each comprising CHCH groups, bonded together in a triangle. We name the corresponding DPD beads aCHCH, to remind that they are part of an aromatic ring. Ether beads are designated as being formed from CH₂OCH₂ or CH₃OCH₂ groups, depending on the location of the bead (central or terminal). Using two bead types for the ethers is essential for reproducing the correct log P for diglyme, for example. Atom to beaded structures are given in detail in Table I.

Having decided on the level of coarse graining, the next part of the model definition is to specify the bonded and non-bonded interactions between beads. For the non-bonded interactions we take the usual DPD pairwise soft repulsion, $\phi = \frac{1}{2} A_{ij} (1 - r/R_{ij})^2$ for $r \leq R_{ij}$ and $\phi = 0$ for $r > R_{ij}$. The values of A_{ij} and R_{ij} are set by the bead types, and the determination of these interaction parameter matrices is the central problem addressed in the present work. Note that unlike much of the existing literature we allow the repulsion ranges to differ from the canonical $R_{ij} \equiv r_c$. As a baseline though we set $R_{ii} = r_c$ and $A = 25$ for the water bead self-repulsion (see discussion in Appendix B).

For the bonded interactions we take an approach motivated by previous work and our own experience. A simple harmonic potential $\phi_b = \frac{1}{2} k_b (r - r_0)^2$ was chosen to represent bonds between connected DPD beads.

The nominal bond length in this (*i. e.* r_0) could be adjusted to reproduce the true experimental distances between groups, and our ambition in future is to do this, however in the present work we adopt a pragmatic approach in which $r_0 = 0.1 \times (N_i + N_j)$ (units of r_c) where N_i and N_j are the number of heavy atoms in beads i and j , respectively (see Table II). A single bond constant $k_b = 150$ was adopted throughout (in units of $k_B T$). Note that, contrary to the usual practice in MD, we (and others) do not exclude the non-bonded interaction between two bonded DPD beads.

Finally, in our model we explicitly introduce an element of rigidity by including a harmonic angular potential between pairs of bonds. This appears to be essential for the correctness of molecular models at the level of coarse graining used here: rigidity has been shown to be important in a number of DPD studies of small molecules (surfactants and lipids), for example surfactant tail stiffness directly controls the surfactant effective length and area-per-molecule [37], and both quantities affect surfactant packing and self-assembly [38]. We here adopt the same three-body angular potential used by Smit and collaborators [37, 39], *viz.* $\phi_a = \frac{1}{2} k_a (\theta - \theta_0)^2$ where θ is the angle between the bonds. In the present work we set $\theta_0 = 180^\circ$ and $k_a = 5$ (in units of $k_B T$) for everything except benzene rings, where instead $\theta_0 = 60^\circ$ (and $k_a = 5$) is used. In this current study we consider only linear or ring (in the case of benzene) molecules.

IV. STAGED PARAMETRIZATION SCHEME

Having specified the model as above, we now turn to the critical task of determining a suitable set of interaction parameters. Here we adopt a staged approach, in which space of undetermined parameters is sequentially refined until we have a single consistent set. This reduces the problem to a manageable sequence of ‘unit operations’.

A. Cutoff distances

In the first step we focus mainly on the cutoff distances R_{ij} . Note that DPD is an example of a ‘mean-field fluid’ and thus there is an element of trade-off between A_{ij} and R_{ij} since the properties are expected to be largely determined by $A_{ij} R_{ij}^3$ [40]. On this basis one could set $R_{ij} \equiv r_c$ for all bead types and attempt to accommodate variation in ‘bead size’ within the A_{ij} matrix. However under the chosen mapping the beads contain different numbers of atoms and do contribute slightly unequally to the total molar volume of the molecules under consideration. As already mentioned therefore, we allow ourselves the flexibility of separately specifying A_{ij} and R_{ij} and use the self repulsion cutoffs R_{ii} to capture, at ‘zeroth order’ as it were, the contribution of the molecular fragments to the overall molar volumes.

TABLE II. Coarse grained (CG) bead content, number of heavy atoms, and molar volumes ($\text{cm}^3 \text{mol}^{-1}$) calculated from Durschlag and Zipper [41]. For water, $N_m = 2$ is the mapping number used to define the DPD length scale r_c .

CG bead	N_i (# heavy atoms)	molar volume
$[\text{H}_2\text{O}]_2$	2 ($\equiv N_m$)	36.0
$[\text{CH}_3]$	1	31.4
$[\text{CH}_2\text{CH}_2]$	2	44.6
$[\text{CH}_2\text{OH}]$	2	33.9
$[\text{aCHCH}]$	2	32.8
$[\text{CH}_2\text{NH}_2]$	2	38.7
$[\text{CH}_2\text{OCH}_2]$	3	50.1
$[\text{CH}_3\text{OCH}_2]$	3	53.2

To do this we used the rules developed by Durschlag and Zipper (DZ) for individual atom contributions to molar volume [41]. We then define R_{ii} such that R_{ii}^3 is proportional to the molar volume of the fragment, with the constant of proportionality being set by the water bead mapping. To deal with the cutoff between dissimilar bead types, we adopt the simple arithmetic ‘mixing rule’ $R_{ij} = \frac{1}{2}(R_{ii} + R_{jj})$. (The observant reader will notice this is equivalent to assigning an effective radius $R_i = R_{ii}/2$ to individual beads, and asserting that $R_{ij} = R_i + R_j$.) Table II presents the molecular fragments used as DPD beads and their corresponding volumes determined by the DZ method and Table III shows the resulting cutoffs. With this first step the cutoffs are now specified (note that no DPD simulations have been undertaken thus far).

B. Self-repulsion

We now turn to the repulsion amplitude matrix A_{ij} . Again taking a pragmatic approach we deal with the self-interaction parameters first, before turning to the repulsion amplitudes between dissimilar bead types. In the second parametrization step therefore we make the initial assumption that $A_{ij} = \frac{1}{2}(A_{ii} + A_{jj})$ and adjust the self-repulsion A_{ii} to fit the experimental densities (at atmospheric pressure and 25°C) of a number of simple molecular liquids containing these beads, computed using the methodology described in Appendix A. With this second step the self-repulsion amplitudes are now fixed.

C. Off-diagonal repulsions

Finally, in the third parametrization step we turn to the repulsion amplitudes between dissimilar bead types (the off-diagonal A_{ij} matrix entries). Here for the first time we target the experimental $\log P$ values, using the computational methodology described in Appendix A. We divide the target molecules into a *training set* of size eight, with a further thirteen used for testing the model.

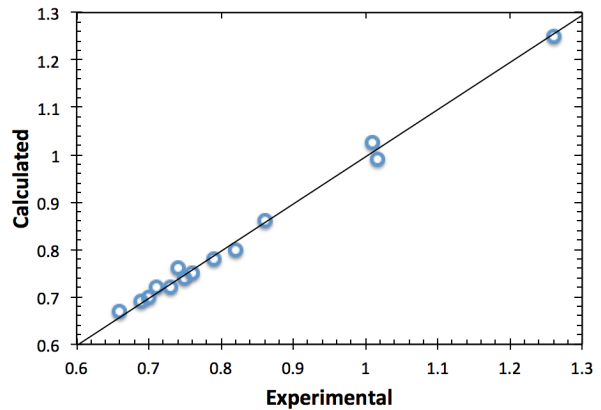


FIG. 1. Experimental versus calculated liquid phase densities. Errors in each calculated result are smaller than the symbols. Units are g cm^{-3} .

As optimization targets we used a combination of water-octanol mutual solubilities and the training set $\log P$ values.

Table IV lists the molecules considered in our $\log P$ study and highlights test versus training solute molecules. The parameters represent the closest fit achieved in terms of the minimum value for root-mean-square error (RMSE) in a manual fitting procedure with a target of 0.3 log units for the training set. Note that the mutual solubilities of water with octanol were both included in the training set. In order to obtain our training set parameters we first optimized A_{ij} for the alcohol molecules to achieve the minimum RMSE for these molecules (note that the self-interactions were held constant at the values determined in the previous, liquid-phase-density-matching step). Following this, whilst holding the alcohol parameters fixed, the amine beads parameters were optimized. The ethers and benzene were dealt with similarly. Table III gives the final set of A_{ij} values resulting from this procedure. In combination with the bonded interaction parameters, this fully specifies the DPD model.

V. RESULTS

Figure 1 compares the calculated densities to the experimental densities for the species used to parametrize self-interaction parameters. The foundation for the fitting of the self-interactions was chosen to be the alkane bead types (CH_2CH_2 and CH_3) as these are present in most solute molecules considered in our work. Hence, multiple alkane molecules were sampled in the parametrization of the self-interaction parameters. Our results for all molecules are in excellent agreement with literature values. The deviations for the alkanes are within 1.5% of the reported values. The trend reproduced by our model slightly over estimates the shorter alkanes

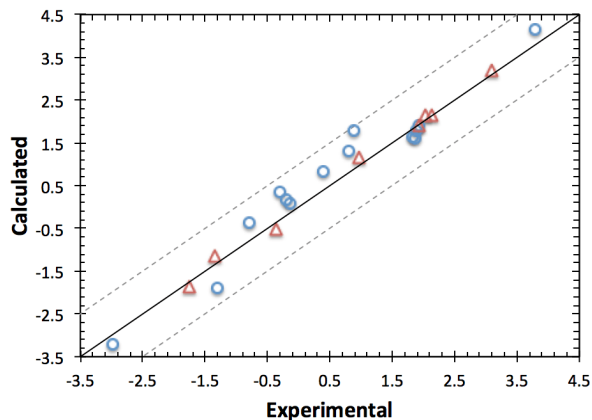


FIG. 2. Experimental versus calculated $\log P$ values. The model has a root-mean-square error (RMSE) of 0.20 log units for the training set (red triangles) and 0.45 log units for the test set (blue circles). Dashed lines represent ± 1 log units.

densities and slightly underestimates at the longer alkane chain lengths. Table V lists the calculated density versus experimental values.

Table IV compares the experimental and calculated $\log P$ values for the solute molecules considered in this study. Overall the calculated $\log P$ values are in good agreement with experimentally determined values, all being within 0.6 log units with the exception of diethyl ether from the test set. Considering the coarseness of the model adopted (manual optimization of parameters, simple model for specifying bond lengths, single angular rigidity), is perhaps a better-than-expected result. The agreement between calculated and experimental $\log P$ values can be observed clearly in Fig. 2. Our model produces a RMSE for of 0.20 and 0.45 log units for our training and test set of molecules, respectively. This is excellent when compared with other predictions of ensembles of solutes (albeit with a small data set in this case).

In setting out an appropriate model for reproducing $\log P$ the most important results to get correct are those of octanol and water themselves (*i. e.* the mutual solubilities). These are therefore very important molecules in our training set. All other calculated results depend upon these values. For example, if there is too much water in the octanol bulk phase then that whole bulk region is too hydrophilic. As a consequence, $\log P$ for other solutes will be skewed. The interaction parameters listed in Table III gives values of 3.2 and -1.1 for octanol and water (logarithm of solubility and inverse solubility, respectively). Experimental values are 3.1 and -1.3 derived from the mutual solubilities reported in Dallos and Liszi [42]. Our results here are the best that were possible with our adopted coarse grained model. Attempts to improve the value for water resulted in poorer values for octanol.

Our hexane model presented a reasonable match to

TABLE III. Repulsion amplitudes (A_{ij}) and cut-off distances (R_{ij}) between all bead pairs in the model (note the letter ‘a’ in ‘aCHCH’ indicates this bead is from an aromatic ring).

bead i	bead j	A_{ij}	R_{ij}
H ₂ O	H ₂ O	25.0	1.0000
H ₂ O	CH ₂ OH	14.5	0.9900
H ₂ O	CH ₂ CH ₂	45.0	1.0370
H ₂ O	CH ₃	45.0	0.9775
H ₂ O	aCHCH	45.0	0.9850
H ₂ O	CH ₂ NH ₂	14.5	1.0120
H ₂ O	CH ₂ OCH ₂	24.0	1.0580
H ₂ O	CH ₃ OCH ₂	32.0	1.0695
CH ₂ OH	CH ₂ OH	14.0	0.9800
CH ₂ OH	CH ₂ CH ₂	26.0	1.0270
CH ₂ OH	CH ₃	26.0	0.9675
CH ₂ OH	aCHCH	27.0	0.9750
CH ₂ OH	CH ₂ NH ₂	18.0	1.0020
CH ₂ OH	CH ₂ OCH ₂	25.0	1.0480
CH ₂ OH	CH ₃ OCH ₂	25.0	1.0595
CH ₂ CH ₂	CH ₂ CH ₂	22.0	1.0740
CH ₂ CH ₂	CH ₃	23.0	1.0145
CH ₂ CH ₂	aCHCH	27.0	1.0220
CH ₂ CH ₂	CH ₂ NH ₂	22.5	1.0490
CH ₂ CH ₂	CH ₂ OCH ₂	28.5	1.0950
CH ₂ CH ₂	CH ₃ OCH ₂	28.5	1.1065
CH ₃	CH ₃	24.0	0.9550
CH ₃	aCHCH	27.0	0.9625
CH ₃	CH ₂ NH ₂	24.0	0.9895
CH ₃	CH ₂ OCH ₂	28.5	1.0355
CH ₃	CH ₃ OCH ₂	28.5	1.0470
aCHCH	aCHCH	27.0	0.9700
aCHCH	CH ₂ NH ₂	27.0	0.9970
CH ₂ NH ₂	CH ₂ NH ₂	21.5	1.0240
CH ₂ OCH ₂	CH ₂ OCH ₂	25.5	1.1160
CH ₂ OCH ₂	CH ₃ OCH ₂	25.5	1.1275
CH ₃ OCH ₂	CH ₃ OCH ₂	25.5	1.1390

literature $\log P$ values, and in benzene we achieved a slightly better match. For the alcohol molecules studied, there is mixed agreement between reported and calculated values. Generally there is good agreement with the longer and di-, tri- and tetra-alcohols fitting the best; this is by construction since in our optimization efforts we focused on the longer molecules for the alcohol functionality. Butanol carries a 0.5 log unit difference. The most notable exception is ethanol with a difference of 0.6 log units, however. Our model presents ethanol as being slightly favoured in the octanol phase as opposed to the water phase. This behaviour could be attributed to an unrealistically favorable interaction between the alcohol functionality bead CH₂OH and the alkane group CH₂CH₂, or, possibly, to increased solubility of water in octanol in our model. This could in turn allow a greater proportion of ethanol to reside in the octanol rich phase. It would appear a potential solution to this could be to make the H₂O/CH₂OH interaction more favorable or the CH₂OH/alkane less favourable. However, both of these approaches has the counter effect of reducing the quality of the fit for the other, longer alcohols (and indeed the all important octanol and water values).

We have sampled six solute molecules that contain ether groups. Whilst our model gives a good fit for

TABLE IV. Experimental versus calculated $\log P$ values for considered solute molecules (in \log_{10} units). The category distinguishes training set molecules (A) from test set molecules (B). The error (defined as standard deviation in the sample mean for $\log P$) in the calculated values is $< 10\%$ of the calculated mean value.

solute	category	$\log P$		$\Delta \log P$
		(expt)	(calc)	
octanol	A	3.1	3.2	0.1
water	A	1.3	1.1	-0.2
hexane	A	3.8	4.1	0.3
ethanol	B	-0.3	0.3	0.6
1-butanol	B	0.8	1.3	0.5
1-hexanol	A	2.0	2.2	0.2
butan-1,4-diol	B	-0.8	-0.4	0.4
glycerol	A	-1.8	-2.0	-0.2
tetritol	B	-3.0	-3.2	-0.2
ethylamine	B	-0.1	0.1	0.2
1-butylamine	A	1.0	1.2	0.2
benzene	A	2.1	2.1	0.0
ethanolamine	B	-1.3	-1.8	-0.5
3-phenyl-1-propanol	B	1.9	1.8	-0.1
3-phenyl-1-propylamine	B	1.8	1.6	-0.2
diethyl ether	B	0.9	1.8	0.9
glyme	B	-0.2	0.2	0.4
diglyme	A	-0.4	-0.5	-0.1
2-(hexyloxy)ethanol	B	1.9	1.6	-0.3
ethyl diglyme	B	0.4	0.8	0.4
benzylmethyl ether	B	1.9	1.9	0.0

TABLE V. Experimental versus calculated densities (g cm^{-3}) for some pure liquids at atmospheric pressure and 25°C . Statistical errors in the calculated values are all in the third decimal place.

species	expt	calc	relative deviation
hexane	0.66	0.67	+1.5 %
octane	0.70	0.70	< 1 %
decane	0.73	0.72	-1.4 %
dodecane	0.75	0.74	-1.3 %
tetradecane	0.76	0.75	-1.3 %
ethanol	0.79	0.78	-1.0 %
octanol	0.82	0.80	-2.5 %
butan-1,4-diol	1.02	0.99	-3.9 %
glycerol	1.26	1.25	-0.7 %
diethyl ether	0.71	0.72	+1.4 %
tetraglyme	1.01	1.04	+3.0 %
ethylamine	0.69	0.69	< 1 %
butylamine	0.74	0.76	+2.7 %
benzene	0.86	0.86	< 1 %

diglyme, 2-(hexyloxy)ethanol and ethyl diglyme, diethyl ether proves to be a poor fit—in fact the poorest fit of all molecules we have considered. This trend of poorer agreement for short molecules and better for long one is again likely due to the fact that we have chosen to fit the ether functionality to a longer molecule (diglyme), for better transferability to longer chains. The fact that our model for diethyl ether is predicted to be much more hydrophobic than in reality, is due to the lower accuracy of our coarse grained model for smaller molecules or

is related to some physics we are neglecting in our simplified model for ethoxylated groups. For diethyl ether our model of a linear molecule may be to blame. It is possible that a better representation of the average conformation is given by a bent trimer, possibly with shorter bonds, which would make it more soluble in water. For the case of glyme, we end up in a situation similar to that of ethanol, in which the DPD determined $\log P$ is of the opposite sign (although the difference from the experimental value is small at 0.4 log units).

In a larger parametrization effort it would be prudent to take into consideration the conformation of the ethoxylated chains. It is known that different conformations of chains, with different relative orientation of the dipole moment centered on the oxygen between adjacent monomers, result in considerably different solvation free energies for the molecule. In particular, a recent combined Raman and density functional theory study [43], has shown that indeed the trans-gauche-trans (tgt) conformation of the molecule has a much larger solvation free energy than the trans-trans-trans (ttt) (which we used to represent the geometry of the coarse-grained dimer), and that population of the (tgt) conformation in water is 79%. It is unclear to us currently whether the simple shortening of the bond length will be enough to represent better glyme, or if instead a better transferability is only possible by including more detailed physics, *e. g.* in the form of an internal degree of freedom for the ether bead or the explicit representation of the ether bead dipole together with a polar model for the coarse-grained water.

Again a trend of better reproduction of the solubility of longer molecules versus shorter ones can be seen for the case of the amines. Butylamine is in good agreement with reported values, and while the difference between reported and calculated for ethylamine is only small, the sign is incorrect. Again, a simple solution might perhaps be to make the amine-water interaction more favourable, but, like in the alcohol case this has further reaching consequences for other solutes. For example, ethanolamine whose $\log P$ is already calculated as too negative by our model. With this latter case we see another short molecule that shows a large deviation from experimental values. Three solutes have been explored that combine benzene functionality in addition to alcohols, amines and ether functionality. All three molecules have reported $\log P$ values in the region of 1.8–1.9 [4, 5]. Our model does a good job are reproducing these values of the three solutes.

Finally, to address the transferability of the model and parameters developed above, the critical micelle concentrations (CMCs) of seven non-ionic surfactants of the C_nE_m family have been calculated as outlined in Appendix A. There is good general agreement between calculated and experimental values across all surfactant molecules explored. These results are pleasing indeed and provide a indication that fitting interaction parameters to $\log P$ values may allow additional properties to be calculated where relative solubility of chemical species

TABLE VI. Experimental versus calculated critical micellisation concentrations (CMCs) (units of wgt %) for seven surfactants of the C_nE_m family. Experimental values have been extracted from several literature sources [44–47]. Number in brackets after calculated result denotes error estimate.

surfactant	CMC (expt)	CMC (calc)
C_6E_4	2	0.8(3)
C_8E_4	0.2	0.2(1)
C_8E_8	0.5	0.3(1)
$C_{10}E_6$	0.04	0.04(2)
$C_{10}E_9$	0.07	0.05(2)
$C_{12}E_6$	0.003	0.008(4)
$C_{12}E_7$	0.003	0.009(5)

play an important role, such as self assembly (micelle formation), phase separation or degree of mixing, and could provide a good basis for larger scale parametrization efforts of models with application to surfactant systems.

VI. DISCUSSION

In this work we have demonstrated that the DPD method can be used to for direct (*i. e.* brute-force) calculation of $\log P$ values for small molecules, and thereby used to parametrize the underlying coarse grained model. We have also shown how to optimize self-interaction parameters and cutoff distances based on bead volumes to give good agreement with experimental liquid phase densities. We stress that we do not expect the interaction parameters to remain valid if the choice of bond length is altered, however. In carrying out the work it has become apparent how to make optimal use of simulation setup for rapid equilibration and to achieve reliable results. The good agreement we have observed between experimental and calculated partition coefficients, and critical micelle concentrations for alkyl ethoxylate surfactants, give us confidence in the resulting parameter set and its transferability. An application to the whole phase diagram of the non-ionic surfactants will be the subject of a forthcoming communication.

Recent work by, for example Lee *et al.*, has focused on parametrizing DPD models by limiting activity coefficients [48]. This should in principle give the same results as the present brute-force method, under the assumption that the force field recovers the same water-octanol phase coexistence compositions. However the equivalence of the two approaches depends crucially upon reproducing exactly the experimental solubility of water in octanol. Even with our very good result (-1.1 vs -1.3 for the logarithm of the mutual solubility of water in octanol), this amounts to $\approx 30\%$ error. Hence the ratio of the mutual limiting activity coefficients of water and octanol bears the same level of error. In practice it appears that for current DPD potential models the two approaches are not exactly equivalent and one has to make a choice on

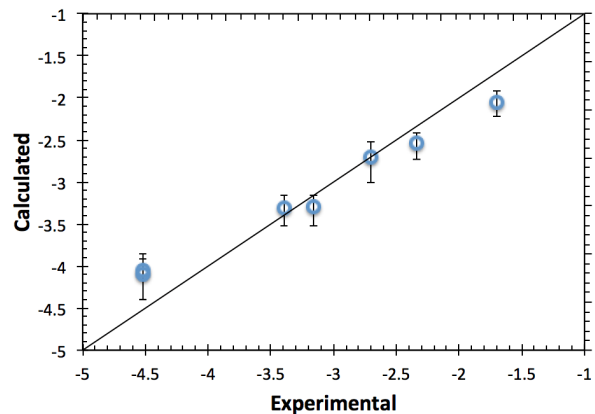


FIG. 3. Experimental versus calculated critical micelle concentrations, CMC, (logarithmic scale, base 10) for selected alkyl ethoxylate surfactants (C_nE_m family). Top right corresponds to molecules with high CMC values, bottom left to low CMC values.

which method to use for parametrization.

We have also determined the limitations of the brute-force calculation of $\log P$, and as such one can envisage extending the approach to incorporate methods inspired by the molecular dynamics studies discussed in the introduction. In particular Monte Carlo methods like Widom insertion could be employed to calculate the transfer free energies, and these are likely to be successful, even for short molecules, for the soft interactions that underpin the DPD model [49]. Also, Gibbs ensemble methods could be employed to generate equilibrated water and octanol phases eliminating the need to control for the presence of an interface. Perhaps most intriguingly, standard Ornstein-Zernike integral equation closures appear to be very accurate for DPD, and perhaps methods developed for molecular liquids such as RISM or SAFT could be applied to calculate phase equilibria and solute partitioning directly for the coarse-grained model [50, 51], provided the appropriate wet octanol model is used to compare with experimental data (correct experimental concentration of water in octanol).

We should also remark that whilst the present approach is presented as a case study in DPD parametrization, it offers a route to calculate *de novo* $\log P$ values. As such it may not be competitive in terms of speed compared to the rapid empirical methods listed in the introduction, but it does appear to be competitive in terms of accuracy [34].

VII. ACKNOWLEDGEMENTS

The authors would like to thank the STFC Hartree Centre for supporting this effort by dedicating human resource and computational infrastructure to this work. RLA and DJB would like to pay particular thanks to Ed

Pyzer Knapp (IBM) and Annalaura Del Regno (STFC) for many stimulating conversations that helped in progressing this work. This work has been partially funded by Innovate UK project 101712 and the authors are grateful to the other members of the UK Computer Aided Formulation (CAF) consortium project for their input and for stimulating discussions.

Appendix A: Methods

We performed DPD simulations using the DL_MESO simulation package [52]. Reduced units are used in which all DPD beads have unit mass, the temperature $k_B T = 1$, and the base length $r_c = 1$ (*i. e.* cutoff for the water bead self interaction). For all simulations a DPD time step of 0.01 (in reduced units) was adopted and trajectory data was collected every 10 DPD time units (1000 time steps).

For an up to date perspective on the DPD methodology see the recent work of Español and Warren [53].

1. Liquid phase densities

In the second optimization step described in the main text, we performed constant pressure (NPT) simulations using the Langevin piston implementation of Jakobsen [54]. The pressure was set to match that of pure water in the model, which corresponds to the pressure in a pure DPD fluid at reduced density $\rho = 3$ and repulsion amplitude $A = 25$. This was determined separately to be $P = 23.7 \pm 0.1$ (in DPD units).

The NPT simulations were carried out for molecules containing alkane, alcohol, amine, ether and benzene moieties, and the self-interaction parameters were varied as described in the main text to reproduce experimental densities of the species investigated (where multiple bead types were present in a test molecule, the arithmetic mixing rule $A_{ij} = \frac{1}{2}(A_{ii} + A_{jj})$ was used as a first approximation). Simulations were run for 300 DPD time units and data collected after the initial 150 DPD time units.

2. Water-octanol partition coefficients

In contrast to the simulations carried out to fit self-interactions to experimental densities, for measuring $\log P$ we carried out constant volume (NVT) simulations. As such initial simulation boxes were constructed so that half of the volume of the simulation cell water filled with water and the other half with octanol. Numbers of beads of each type were selected in order to achieve the desired system-wide target pressure of $P = 23.7$. This is important to maintain the correct density of the two solvent phases.

Four simulation box sizes were adopted in the calculation of $\log P$, where each was a multiple of a basic

$60 \times 20 \times 20$ box. These are listed in Table VII. The largest of these ('huge') corresponds to 1.2×10^6 beads in total. For the 'small' simulations, the left part of the box (the region $0 < x < 30$) was populated by 36 000 water beads and the right part ($30 < x < 60$) by 7800 octanol molecules (39 000 beads). The total number of beads therefore being 75 000. For the larger boxes the small box was replicated in the y and z dimensions as required. Therefore, the simulation begins with water and octanol partitioned into their respective pure phases. Solute molecules were added by random insertion into the simulation box. The number of water molecules and octanol molecules are correspondingly adjusted to account for the presence of solute molecules. By following this approach all of our simulations were performed within 2% of the target pressure with the exception of glycerol and tetritol which had pressures within 5% of the target value. The initial configurations were created using the PACKMOL package [55].

Different box sizes are required to cover different $\log P$ ranges. A simple estimate suggests the maximum achievable $\log P$ range, for a given simulation box size. For example, in a 'small' box containing 5% solute beads, there are a total of 3750 solute beads. Assuming a solute molecule comprises of 3 beads, and supposing that of order one molecule should be present in the *disfavourable* phase at all times, this corresponds to a maximum achievable range of $\log P = \pm \log_{10}(3750/3) \approx \pm 3$. However, we have found in practice this overestimates the accessible $\log P$ range. Our empirically determined limits for a reliable $\log P$ calculation (with 5% solute beads) are given as the second column in Table VII. With these limitations sampling errors can be kept at a sensible level ($< 10\%$ of the calculated mean solute concentration).

The effect of the solute concentration upon calculated $\log P$ quality and equilibration time was also explored. Trial simulations of 1–5% solute were carried out. Given that the number of solute molecules present in the box defines the maximum limit for $\log P$ (as discussed above) it is preferential to have a large as possible value for the solute concentration in the simulation. In addition, with larger solute concentrations, shorter simulations can be carried out. However, a too high value may adversely effect the integrity of the bulk phases (*e. g.* by spontaneous phase separation of the solute) making any calculated $\log P$ worthless.

A number of different options were trialled for initial solute molecule placement: completely random (with 50 : 50 mix in both solvents), all in octanol, or all in water. In all cases particles were randomly spread within the specified region. Positioning solute molecules close to the interface was also trialled. We have found that the ideal initial positioning of the solute depends upon the target $\log P$. Whilst unsurprising, there are important consequences to this. If, for example, glycerol is placed in any reasonably large concentration in the octanol phase (supposing that the solute is randomly distributed), it will spontaneously phase separate in this phase. This

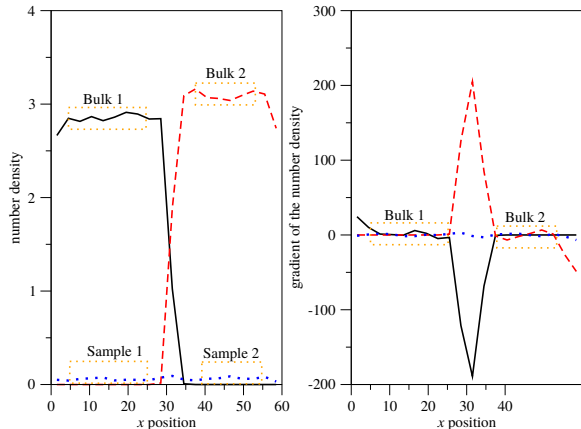


FIG. 4. Evaluating the region of interface and two bulk phases. The left subplot shows 1D number density profile for water (solid line) and octanol (dashed-line). The right subplot shows the gradient in number density for the equivalent profiles. A bulk phase is defined where the gradient varies by no more than $\pm\epsilon$ over more than one sample point (where $\epsilon = 0.05$), with two such highlighted here by the dotted boxes. Regions that lie outside this are assumed to represent interfaces.

has a big impact on the calculated $\log P$ value because the system does not equilibrate over a feasible time scale. In our trials for example we found the glycerol $\log P$ value fluctuates wildly if the solute molecules are not initially positioned in the bulk water region. Obviously if a simulation is allowed to run long enough then the problem resolves itself, however, this is not efficient for high throughput simulations for parametrization.

Throughout the course of our study, it was found that simulations only needed to be run for a maximum of 20 000 DPD time units to meet the criteria for equilibration and data collection of $\log P$ values for the ‘small’ and ‘medium’ box sizes. Larger boxes are used for higher $\log P$ values and as such the actual number of steps to reach equilibrium was larger and typically took around 30 000 DPD time units. Indicative run times for the typical $\log P$ calculations are given in the final columns of Table VII.

We turn now to the methodology of extracting $\log P$ values from simulation data. In this work we calculate the value of $\log P$ for a molecule by direct application of Eq. (1), using computed values of the solute concentrations in octanol and water phases. For each case we undertook the following procedure:

1. Calculate the 1D number density profile running along the x -axis (*i. e.* normal to the interface), see left pane of Fig. 4.
2. Determine where the interface lies along x .

TABLE VII. Simulation box sizes used in $\log P$ calculations. The second column indicates the range of $\log P$ values accessible to brute-force simulation. The indicative run times correspond to the given resource allocation (cores) on an IBM NextScale system (2×12 core Intel Xeon processors; Ivy Bridge E5-2697v2 2.7 GHz; 64 GB RAM).

box size	$\log P$	run time	cores
$60 \times 20 \times 20$ (small)	± 2.0	2 hrs	96
$60 \times 40 \times 40$ (medium)	± 2.5	3 hrs	144
$60 \times 60 \times 60$ (large)	± 3.5	5 hrs	240
$60 \times 80 \times 80$ (huge)	± 4.0	6 hrs	512

3. Determine the bulk solvent boundary x -positions and corresponding length of the bulk phase of water and octanol excluding the transitioning interface. These regions should be mutually exclusive.
4. Calculate the average number of solute molecules within these two bulk regions. These provide our estimates of the mean number density of solute within the water and octanol phases.
5. Calculate the ratio of these number densities to obtain $\log P$ from Eq. (1).

In calculating the mean solute concentrations the interface region between octanol and water was excluded to ensure only the bulk phase concentrations should be considered, analogous to experiment. To facilitate this the following algorithm was developed to automatically identify the interface region. We first take the time-averaged 1D number density profiles of water and of octanol and calculate the gradient of these (see right pane of Fig. 4). The regions where the gradient fluctuates around zero define the bulk phases. The interface region can be identified by looking for a spike (positive or negative) in the gradient that is an order of magnitude greater than the fluctuations seen in the bulk regions. This spike defines the interface region to be excluded from number density calculations. The left-hand pane of Fig. 4 shows how the number density of the two bulk solvents varies along the x -axis. The regions over which the solute concentration value can be calculated is highlighted for each bulk solvent. Estimates for the number density of solute within bulk phase were calculated by taking the mean value within the boundaries of each bulk region (labelled Sample 1 and Sample 2 in Fig. 4).

To estimate the error in $\log P$ calculated in this way, we use block averaging of the time series of $\log P$ obtained from the instantaneous mean solute concentrations from the recorded trajectory (*i. e.* every 10 DPD time units). The block size is 100 DPD time units (10 measurements), and we average over 100 blocks to obtain a sample mean value for the block. The reported errors represent the standard deviation in the calculated sample means over the whole data collection period.

There are three important considerations in tuning our methods for calculating $\log P$: handling poor parameter choice, poor equilibration, and poor sampling of solute concentrations. We discuss each of these in turn.

Handling poor parameter choice — During the tuning of the model interaction parameters to fit the $\log P$ of our test set there was the potential for the bulk water-octanol phases to break down due to poorly chosen model parameters. If the parameters were good then there would be only two bulk phases (corresponding to how we constructed the initial systems). If the parameters were poor then either a single phase would be found, which suggests that water and octanol had completely mixed, or more than two bulk phases would be identified which suggested that some kind of microphase separation might be happening. Only when two distinct bulk phases are present can the $\log P$ calculation be estimated with confidence using our methodology.

Poor equilibration — Simulations were started with molecular configurations that may be far from equilibrium with respect to $\log P$, such as uniformly dispersed solute molecules for example. Over time, the solute molecules migrate to their preferred phase and during that period the estimated value of $\log P$ value will change. Obviously for obtaining thermodynamic averages, data should not be used until the system has equilibrated. In this work systems were considered equilibrated after the estimated value of $\log P$ remained stable over 100 blocks of time (where as above each block is 100 DPD time units). The choice of 100 blocks was determined somewhat arbitrarily, but seems to represent a good choice for the systems and system sizes considered in this work. Data was collected for 10000 DPD time units following equilibration (with particle data collected once every 10 DPD time units) in order to determine the average (sample mean) $\log P$ value for a particular system. If the standard deviation of a particular $\log P$ was $> 10\%$ of the mean value we considered the value to be void and sampled the system in a larger simulation box to reduce error. We discuss typical equilibration times in the results section for each of the simulation box sizes considered. As discussed in the previous section, when the simulation box is comparably small relative to the true $\log P$, all the solute could tend to accumulate in one of the solvents. In these cases we rejected the results of the calculations and re-ran the simulation in a larger simulation box.

Poor sampling — To calculate $\log P$ reliably from our simulations it is important to ensure good sampling, and therefore get good estimates, of the mean solute concentrations. This is essentially a problem of counting statistics, and critically depends on the number of solute molecules in the *disfavourable* phase. It provides practical limits on the overall solute concentration, and on the $\log P$ range that can be measured for a given simulation box size. Pragmatically we found that reliable estimates can be obtained for $\log P$ using the above block averaging scheme (over 100 blocks of 10 DPD time units), using 5%

solute concentration, provided that we specify if the standard deviation is greater than 10% of the sample mean of the $\log P$ we reject the measurement and re-do the calculation in the next larger simulation box. A 5% solute concentration (*i. e.* 5% of beads in the box comprise the solute molecules) equates to a mole fraction of 0.025 for the smallest molecule we consider (2 beads) and 0.01 for the largest (5 beads). Should large molecules be sampled, which comprise a large number of beads, there may be insufficient solute material to achieve good sampling. We recommend that mole fraction values be in the range of that specified above for further fitting.

3. Critical micelle concentrations

Constant pressure simulations were performed to calculate the CMC of seven non-ionic surfactants of the C_nE_m family. Specifically, C_6E_4 , C_8E_4 , C_8E_8 , $C_{10}E_6$, $C_{10}E_9$, $C_{12}E_6$ and $C_{12}E_7$ surfactants were explored. Simulation boxes contained 325 000 DPD beads and were run for 30 000 DPD time units. The initial 1/3 of simulation time was used for equilibration and the subsequent 2/3 for data collection. The CMC was extracted adopting the method outlined in Johnston *et al.* [56].

Appendix B: Note on compressibility matching

The baseline choice $A = 25$ for the water bead repulsion amplitude originated in the seminal work of Groot and Warren [57], who attempted to match the compressibility of DPD water to that of ‘real’ water. It was later found that there was a missing factor of the mapping number N_m , so that for a correct compressibility matching one should use $A \approx 26 N_m$ (see below) [58]. Since our preference is not to do this, a few words of explanation are warranted. We first note that a large value of the baseline repulsion leads to increased solvent structuring, which can be regarded as a discretization artifact of the coarse grained model. Indeed, if $A \gtrsim 200$ the DPD solvent ‘freezes’ (most likely into a BCC structure) [59]. Thus we should prefer to use a small baseline repulsion amplitude; the question is: how small?

To answer this, recall that from statistical mechanics the relative mean square density fluctuations in a volume V are $\langle \Delta \rho^2 \rangle / \rho^2 = \kappa_T k_B T / V$ where $\kappa_T^{-1} = \rho \partial p / \partial \rho$ is the (inverse) isothermal compressibility. Thus relative density fluctuations are inversely proportional to the sample volume, and for liquid water at room temperature the coefficient of proportionality $\kappa_T k_B T \approx 1.9 \text{ \AA}^3$. For DPD the same quantity is also well defined. Assuming the equation of state $p \approx \alpha A \rho^2$ with $\alpha \approx 0.101$ [57] (*i. e.* neglecting the ideal contribution which is small), one has $\kappa_T k_B T \approx 1 / (2\alpha A \rho^2)$, in DPD units. Recalling that $\rho N_m v_m \equiv 1$ one finally has the formal mapping $\kappa_T k_B T = N_m v_m / (2\alpha A \rho_c^3)$. Making the standard choice

$\rho r_c^3 = 3$ and inserting the actual numbers for water arrives at $A \approx 26 N_m$ as claimed.

The argument could obviously be extended to match compressibility, and hence density fluctuations, for other molecular liquids. However, rather than insisting that the compressibility be exactly matched as in earlier works, we here argue what really matters is that density fluctuations should be relatively insignificant *above the*

DPD length scale. For example in water $\langle \Delta \rho^2 \rangle / \rho^2 \lesssim 0.01$ for $V \gtrsim r_c^3 \approx 180 \text{ \AA}^3$. To ensure that the relative density fluctuations in the DPD water model are bounded by $\langle \Delta \rho^2 \rangle / \rho^2 \lesssim 0.05$ (for example), requires only that $1/2\alpha A \rho^2 \lesssim 0.05$, or $A \gtrsim 10$ for standard DPD. This is satisfied for our purposes for all our bead types.

-
- [1] A. Leo, C. Hansch, and D. Elkins, *Chem. Rev.* **71**, 525 (1971).
- [2] J. Sangster, *Octanol-water partition coefficients*, 1st ed. (Wiley, 1997).
- [3] H. J. Heipieper, F. J. Weber, J. Sikkema, H. Keweloh, and J. A. de Bont, *Trends Biotechnol.* **12**, 409 (1994).
- [4] J. Sangster, *J. Phys. Chem. Ref. Data* **18**, 1111 (1989).
- [5] <http://www.chemspider.com> (2017).
- [6] B. Beck, A. Breindl, and T. Clark, *J. Chem. Inf. Comput. Sci.* **40**, 1046 (2000).
- [7] P. Duchowicz, E. Castro, A. Toropov, I. Nesterov, and O. Nabiev, *Molec. Divers.* **8**, 325 (2004).
- [8] A. K. Ghose, V. N. Viswanadhan, and J. J. Wendoloski, *J. Phys. Chem. A* **102**, 3762 (1998).
- [9] A. Stenzel, K.-U. Goss, and S. Endo, *Environ. Toxicol. Chem.* **33**, 1537 (2014).
- [10] M. Buggert, C. Cadena, L. Mokrushina, I. Smirnova, E. J. Maginn, and W. Arlt, *Chem. Eng. Technol.* **32**, 977 (2009).
- [11] A. Loschen, Christoph Klamt, *Ind. Eng. Chem. Res.* **53**, 11478 (2014).
- [12] S. J. Marrink and D. P. Tieleman, *Chem. Soc. Rev.* **42**, 6801 (2013).
- [13] S. Genheden, *J. Chem. Theory Comput.* **12**, 297 (2016).
- [14] N. Bhatnagar, G. Kamath, I. Chelst, and J. J. Potoff, *J. Chem. Phys.* **137**, 014502 (2012).
- [15] G. Kamath, N. Bhatnagar, G. A. Baker, S. N. Baker, and J. J. Potoff, *Phys. Chem. Chem. Phys.* **14**, 4339 (2012).
- [16] N. Bhatnagar, G. Kamath, and J. J. Potoff, *Phys. Chem. Chem. Phys.* **15**, 6467 (2013).
- [17] N. M. Garrido, I. G. Economou, A. J. Queimada, M. Jorge, and E. A. Macedo, *AIChe J.* **58**, 1929 (2011).
- [18] P. Yamin, R. Isele-Holder, and K. Leonhard, *Ind. Eng. Chem. Res.* **55**, 4782 (2016).
- [19] T. Bereau and K. Kremer, *J. Chem. Theory Comput.* **11**, 2783 (2015).
- [20] J. W. Essex, C. A. Reynolds, and W. G. Richards, *J. Am. Chem. Soc.* **114**, 3634 (1992).
- [21] N. M. Garrido, M. Jorge, A. J. Queimada, E. A. Macedo, and I. G. Economou, *Phys. Chem. Chem. Phys.* **13**, 9155 (2011).
- [22] N. M. Garrido, A. J. Queimada, M. Jorge, E. A. Macedo, and I. G. Economou, *J. Chem. Theory Comput.* **5**, 2436 (2009).
- [23] N. M. Garrido, I. G. Economou, A. J. Queimada, M. Jorge, and E. A. Macedo, *AIChe J.* **58**, 1929 (2012).
- [24] A. P. Lyubartsev, S. P. Jacobsson, G. Sundholm, and A. Laaksonen, *J. Phys. Chem. B* **105**, 7775 (2001).
- [25] A. S. Paluch, J. K. Shah, and E. J. Maginn, *J. Chem. Theory Comput.* **7**, 1394 (2011).
- [26] A. S. Paluch, D. L. Mobley, and E. J. Maginn, *J. Chem. Theory Comput.* **7**, 2910 (2011).
- [27] B. Chen and J. I. Siepmann, *J. Am. Chem. Soc.* **122**, 6464 (2000).
- [28] B. Chen and J. I. Siepmann, *J. Phys. Chem. B* **110**, 3555 (2006).
- [29] C. C. Bannan, G. Calabro, D. Y. Kyu, and D. L. Mobley, *J. Chem. Theory Comput.* **12**, 4015 (2016).
- [30] J. Michel, M. Orsi, and J. W. Essex, *J. Phys. Chem. B* **112**, 657 (2008).
- [31] A. Pohorille, C. Jarzynski, and C. Chipot, *J. Phys. Chem. B* **114**, 10235 (2010).
- [32] C. D. Christ, A. E. Mark, and W. F. van Gunsteren, *J. Comput. Chem.* **31**, 1569 (2010).
- [33] C. Chipot and A. Pohorille, *Free Energy Calculations: Theory and Applications in Chemistry and Biology* (Wiley, 2007).
- [34] J. G. E. M. Fraaije, J. van Male, P. Becherer, and R. Serral Gracia, *J. Chem. Inf. Model.* **56**, 2361 (2016).
- [35] B. Widom, *J. Chem. Phys.* **39**, 2808 (1963).
- [36] D. Frenkel and B. Smit, *Understanding molecular simulation*, 2nd ed. (Academic Press, 2001).
- [37] M. Venturoli and B. Smit, *Phys. Chem. Comm.* **2**, 45 (1999).
- [38] R. Nagarajan, *Langmuir* **18**, 31 (2002).
- [39] M. Venturoli, M. M. Sperotto, M. Kranenburg, and B. Smit, *Phys. Rep.* **437**, 1–54 (2006).
- [40] A. A. Louis, P. G. Bolhuis, and J. P. Hansen, *Phys. Rev. E* **62**, 7961 (2000).
- [41] P. Durchschlag, H. Zipper, *Prog. Colloid. Polym. Sci.* **94**, 20 (1994).
- [42] A. Dallos and J. Liszi, *J. Chem. Thermodyn.* **27**, 447 (1995).
- [43] R. Wada, K. Fujimoto, and M. Kato, *J. Phys. Chem. B* **118**, 12223 (2014).
- [44] <https://www.anatrace.com> (2017).
- [45] J. M. Corkill, J. F. Goodman, and S. P. Harrold, *Trans. Faraday Soc.* **60**, 202 (1964).
- [46] M. Frindi, B. Michels, and R. Zana, *J. Phys. Chem.* **96**, 6095 (1992).
- [47] M. J. Schick, *Nonionic surfactants*, 1st ed. (Marcel Dekker, 1987).
- [48] M.-T. Lee, R. Mao, A. Vishnyakov, and A. V. Neimark, *J. Phys. Chem. B* **120**, 4980 (2016).
- [49] C. M. Wijmans, B. Smit, and R. D. Groot, *J. Chem. Phys.* **114**, 7644 (2001).
- [50] E. L. Ratkova, D. S. Palmer, and M. V. Fedorov, *Chem. Rev.* **115**, 6312 (2015).
- [51] W. G. Chapman, K. E. Gubbins, G. Jackson, and M. Radosz, *Ind. Eng. Chem. Res.* **29**, 1709 (1990).
- [52] M. A. Seaton, R. L. Anderson, S. Metz, and W. Smith, *Mol. Simulat.* **39**, 796 (2013).

- [53] P. Español and P. B. Warren, *J. Chem. Phys.* **146**, 150901 (2017).
- [54] A. F. Jakobsen, *J. Chem. Phys.* **122**, 124901 (2005).
- [55] L. Martinez, R. Andrade, E. G. Birgin, and J. M. Martinez, *J. Comput. Chem.* **30**, 2157 (2009).
- [56] M. A. Johnston, W. C. Swope, K. E. Jordan, P. B. Warren, M. G. Noro, D. J. Bray, and R. L. Anderson, *J. Phys. Chem. B* **120**, 6337 (2016).
- [57] R. D. Groot and P. B. Warren, *J. Chem. Phys.* **107**, 4423 (1997).
- [58] R. Groot and K. Rabone, *Biophys. J.* **81**, 725 (2001).
- [59] A. Lang, C. N. Likos, M. Watzlawek, and H. Löwen, *J. Phys. Condens. Matter* **12**, 5087 (2000).